MRS Advances © 2018 Materials Research Society
DOI: 10.1557/adv.2018.520

High Performance Tin-coated Vertically Aligned Carbon Nanofiber Array Anode for Lithium-ion Batteries

Gaind P. Pandey[1], Kobi Jones[1], Emery Brown[2], Jun Li[2] and Lamartine Meda[1]

[1]*Department of Chemistry, Xavier University of Louisiana, New Orleans, LA 70125*

[2]*Department of Chemistry, Kansas State University, Manhattan, KS 66506*

ABSTRACT

This study reports a high-performance tin (Sn)-coated vertically aligned carbon nanofiber array anode for lithium-ion batteries. The array electrodes have been prepared by coaxial sputter-coating of tin (Sn) shells on vertically aligned carbon nanofiber (VACNF) cores. The robust brush-like highly conductive VACNFs effectively connect high-capacity Sn shells for lithium-ion storage. A high specific capacity of 815 mAh g^{-1} of Sn was obtained at C/20 rate, reaching toward the maximum value of Sn. However, the electrode shows poor cycling performance with conventional $LiPF_6$ based organic electrolyte. The addition of fluoroethylene carbonate (FEC) improve the performance significantly and the Sn-coated VACNFs anode shows stable cycling performance. The Sn-coated VACNF array anodes exhibit outstanding capacity retention in the half-cell tests with electrolyte containing 10 wt.% FEC and could deliver a reversible capacity of 480 mAh g^{-1} after 50 cycles at C/3 rate.

INTRODUCTION

To meet the increasing demands of high-energy density lithium-ion batteries (LIBs) for electric vehicles and energy storage systems several higher capacity anode materials such as lithium (Li), silicon (Si), germanium (Ge) and tin (Sn) have been studied to replace the graphite currently used in the commercial LIBs [1-3]. Among Li-alloying anodes (Si, Ge, Sn etc.), Sn recently has been considered as a promising anode material because of the high theoretical specific capacity of 994 mAh g^{-1} for its alloy

$Li_{22}Sn_5$ [4, 5]. Although its abundant nature makes Sn an attractive anode material, the application of Sn as an anode is still far from realization. One of the critical issues is the huge volume expansion (>300%) and aggregation of Sn nanoparticles during lithium alloying (insertion) and dealloying (extraction) processes and, hence induces severe anisotropic stress, leading to particle pulverization, solid electrolyte interphase (SEI) destabilization, and consequently fast capacity fading in the initial cycles [3].

Various nanostructured Sn materials including nanoparticles, nanowires, and nano-sheets have been developed to reduce the internal stress and to make use of their large specific surface area and short Li^+ diffusion length in solids [3-5]. Various forms of carbon materials have also been incorporated with nanostructured Sn to form composite anode materials. Here we demonstrate the hybrid core-shell nanofibers utilizing a highly conductive and stable vertically align nanofiber core to support a coaxial Sn shell as a LIB anode in a unique vertical 3D architecture.

EXPERIMENTAL DETAILS

Copper foils (84 μm, Copper 102, Hamilton Precision Metals, PA) were coated with a 300 nm thick chromium barrier layer, followed by a 30 nm nickel catalyst layer using a high-vacuum PerkinElmer 4400 series magnetron sputtering system at the UHV Sputtering Inc. (Morgan Hill, CA). The Cr/Ni coated Cu sheets were then cut into ~17.5 mm diameter disks to grow VACNFs with an average length of ~5 μm using a DC-biased plasma enhanced chemical vapor deposition (PECVD) system (AIXTRON, CA, USA) following a procedure reported in the literature [6-8]. In brief, a pretreatment procedure was applied by thermally heating the substrate to 500 °C in 250 sccm NH_3 at a pressure of 3.9 Torr, followed with a 40 W plasma treatment for 60 s. The combined effects of thermal dewetting and NH_3 plasma etching broke down the Ni film into randomly distributed nanoparticles that catalyzed the growth of VACNFs in a tip growth mode [6, 7]. Following the pretreatment, a mixture of acetylene (70 sccm) and NH_3 (250 sccm) was introduced as the precursor at 750 °C and a pressure of 4.6 Torr. The plasma power was kept at 45 W for 30 min to grow ~ 5.0 μm long VACNFs. Pure Sn was deposited on VACNF arrays to form the VACNF-Sn core-shell nanostructure using a Denton Vacuum (Desktop PRO) by RF magnetron sputtering in which a Sn target (99.999%) was sputtered at 20 W under pure Argon atmosphere with a deposition rate of 10-12 nm per min. The nominal thickness of Sn was measured on a flat Si wafer surface by FE-SEM. SEM micrographs of VACNFs and VACNF-Sn core-shell nanostructures were collected on a Hitachi field-emission scanning electron microscope (Model: S-4800) at a working distance of 7-8 mm and accelerating voltage of 10 kV at 45° perspective views.

To evaluate the electrochemical performance of the VACNF-Sn core-shell array anode half cells were assembled into stainless steel coin cells (CR2032-type) in an argon-filled glove box (MBraun LabStar, USA) containing less than 0.5 ppm of H_2O or O_2. The VACNFs-Sn were used as the working electrode against a pure lithium disk as the counter electrode. The coin cells were assembled with glass fiber separator soaked with electrolyte solution of a 1.0 M lithium hexafluorophosphate ($LiPF_6$) in a mixture of ethylene carbonate (EC) and dimethyl carbonate (DMC) in 1:1 volume ratio with and without 10 wt.% of fluoroethylene carbonate (FEC) (Sigma-Aldrich, USA). Cyclic voltammetry (CV) was performed in the potential range of 0.05-1.5 V versus Li/Li^+ at 0.1 mV s^{-1} scan rate. Galvanostatic charge-discharge cycling was performed at room temperature and operated at voltages of 0.05-1.5 V versus Li/Li^+ using an Arbin cell test system (BT-2000; Arbin Instruments, USA). The gravimetric capacity was calculated by dividing only the mass of Sn over the electrode surface, which was calculated from the nominal thickness measured by FE-SEM at the cleaved cross-section of a reference Si

wafer (~ 600 nm) and the density of sputtered tin (7.31 g cm^{-3}). The sputtered Sn mass on VACNFs was ~1.14 mg on ~2.4 cm^2 disk.

RESULTS AND DISCUSSION

The vertically aligned carbon nanofiber (VACNF) arrays on Cu foil grown by PECVD have been utilized to coaxially coat Sn shells. Figure 1a shows the SEM images of an as-grown VACNF array on a Cu foil and Sn coated VACNF array anode. The CNFs are firmly attached to the Cu foil substrates and provide a highly conductive electron pathway between the current collector and active Sn shell. The conductivity of CNFs is 2.5×10^3 S cm^{-1} [9]. The SEM images of Sn-coated VACNFs, in figure 1 (b and c), indicate that Sn form coaxial shells with a large mass at the fiber tips that tapers gradually down to the CNF base. The grain size of the coated Sn is in the range of 10-20 nm. Such nanostructure can effectively accommodate the volume expansion/contraction of Sn in the radial direction during charge-discharge cycles. The power density is also expected to improve significantly due to the short path of Li^+ transport across the Sn shell with smaller grain size. Figures 1d depicts SEM image of the electrode disassembled after half-cell charge-discharge test from the coin-cells. The cell was stopped at lithiated (discharged) state to disassemble. The Sn grains are covered by the SEI layer formed over the Sn surface which can be observed clearly (figure 1d). The 3D core-shell structure of electrode remained stable during both cell assembly and electrochemical test.

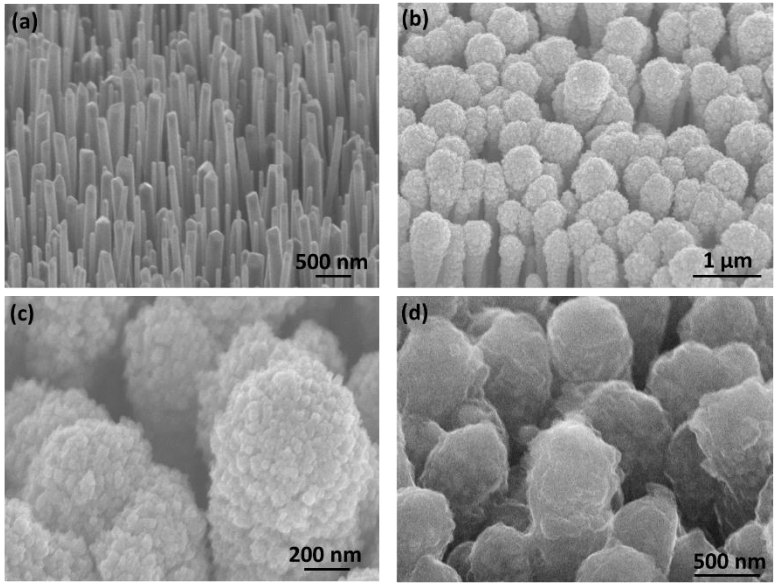

Figure 1. Representative SEM images of (a) an as-grown VACNF array; (b and c) a similar VACNF array after sputter coating with Sn (thickness of ~600 nm) and, (d) VACNF-Sn array electrode after half-cell charge-discharge cycles.

The electrochemical performance of the Sn coated VACNF array anode has been carried out by CV and charge-discharge method in the half-cell configuration. Figure 2a shows the cyclic voltammograms of a representative half-cell at scan rate 0.1

mV s^{-1}. In the first cathodic scan, the peaks positioned between 0.65 to 0.15 V are represented alloying process of lithium into tin forming Li_xSn and solid electrolyte layer formation. In the anodic scan, a series of peaks between 0.4 and 0.8 V (0.49, 0.64, 0.74, 0.80 V) are assigned to the de-alloying reaction of Li_xSn [10]. The CV curves of the second and third scans are almost overlapped, indicating that good electrochemical reversibility of lithium storage in the VACNF-Sn array anode starts from the second cycle. It can be seen that the CNF arrays have negligible contribution as no observable peak formed in lithium intercalation into carbon below 0.15 V. The voltage profiles of the VACNFs-Sn half-cell in the 1, 3, 4 and 6th galvanostatic cycles at the C/20 (1 and 3) and C/10 (4 and 6) rates are shown in figure 2b. The specific capacity was calculated using the mass of coated Sn. The referred C-rates are based on the theoretical specific capacity of the Sn ~994 mAh g^{-1}. In the first cycle, the insertion and extraction capacities reached 1035 and 836 mAh g^{-1}, respectively, and the Coulombic efficiency is ~ 81%. The low efficiency for the first cycle can be mainly due to the excess reaction in the Li insertion process associated with the formation of an irreversible SEI layer at the Sn surface and other irreversible side reactions, which is common in metal alloying anodes. However, the third cycle showed insertion and extraction capacities of 815 and 781 mAh g^{-1}, respectively, with coulombic efficiency jumping up to ~95.8% indicating a good electrochemical reversibility of lithium storage.

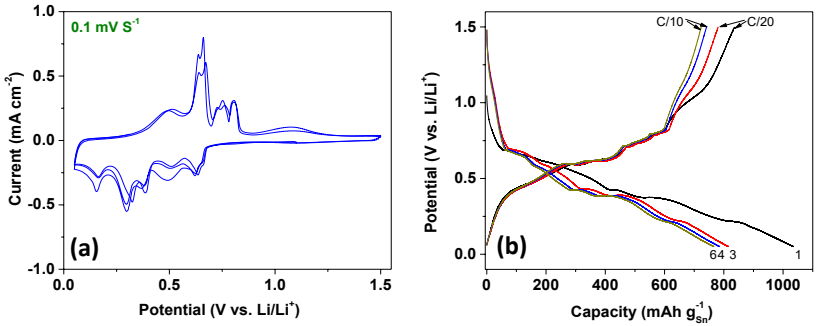

Figure 2. (a) Cyclic voltammogram of a VACNF-Sn electrode at the scan rate of 0.1 mV s^{-1}. (b) The voltage profiles of the 1, 3, 4 and 6th galvanostatic charge-discharge cycles of the half-cell at the C/20 (1 and 3) and C/10 (4 and 6) rates (C rate is calculated based on the theoretical capacity of Sn ~ 994 mAh g^{-1}).

To evaluate the cycling performance of the VACNF-Sn array anode, galvanostatic charge-discharge measurements at C/3 rate were carried out. The insertion/extraction capacity and coulombic efficiency versus cycle numbers for both half-cells with and without FEC containing $LiPF_6$ based organic electrolyte are presented in figures 3(a & b) and 3(c & d) , respectively. Although the VACNF-Sn array electrode delivered a high capacity during early cycles, there was an abrupt onset of capacity fade at cycle 15 (figure 3a and b). The loss of electrochemical capacity is related to the poor SEI stability formed on Sn surface during prolonged electrochemical cycling [11]. To investigate the effect of electrolyte additives on the electrochemical performance of VACNF-Sn array anode, half-cell with 10 wt.% FEC in the $LiPF_6$ based electrolyte was galvanostatically cycled at C/3 rate, as shown in the figure 3c. The cell containing FEC shows similar capacity retention in the first 15 cycles, showing that the addition of FEC does not improve the capacity retention in the initial charge-discharge cycle, significantly. However, a distinct trend can be seen after initial cycles as capacity retention is improved significantly in the long-term cycling (figure 3c and d).

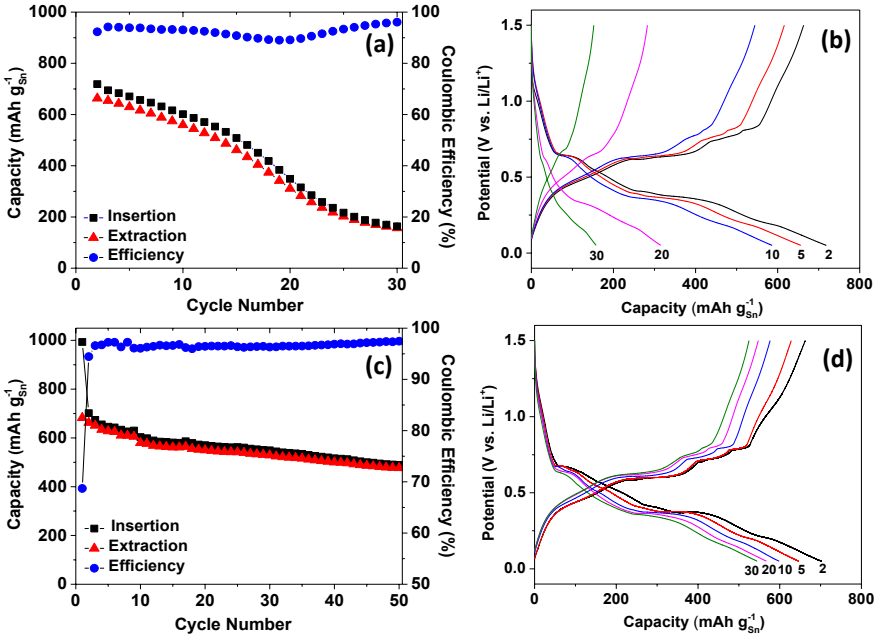

Figure 3. (a) Cycling performance of the VACNF-Sn array anode with a base electrolyte solution at C/3 rate and (b) Galvanostatic charge-discharge profiles at different cycle numbers (mentioned in figure) of this half-cell. (c) Cycling performance of the VACNF-Sn array anode with an electrolyte solution with 10 wt.% FEC as an additive at C/3 rate and (d) Galvanostatic charge-discharge profiles at different cycle numbers (mentioned in figure) of this half-cell.

Table I. Comparison of the VACNFs-Sn electrode performance with literature.

Electrode	Electrolyte	Cycle Number	Capacity (mAh g^{-1})	Reference
Sn-coated VACNT	1 M $LiPF_6$ in EC/DMC (1:1 v/v)	1000	400 (C/2 rate)	5
Sn/porous Cu foam	1.2 M $LiPF_6$ in EC: EMC (3:7 w/w) + 10% FEC	50	-	11
F-doped Sn-Ni film	1 M $LiPF_6$ in FEC:DEC (1:1 v/v)	50	442-406	12
Sn nanoparticles (slurry coating)	1.2 M $LiPF_6$ in EC: EMC (3:7 w/w) + 5 or 10% FEC (or 5% VC)	50	~500	13
3D SnO_2/graphene foam	1 M $LiPF_6$ in EC/DMC (1:1 v/v)	150	534	14
SnO_2 in carbon matrix	1 M $LiPF_6$ in EC/DMC/EMC (1:1:1 v/v/v)	400	608	15
Sn in CNFs matrix	77.5Li_2S-22.5P_2S glass electrolyte	50	762 (C/20 rate)	16
VACNFs-Sn	1 M $LiPF_6$ in EC/DMC (1:1 v/v)+10% FEC	50	600-480 (C/3 rate)	Present work

The addition of FEC in the $LiPF_6$ based electrolyte also improves the coulombic efficiency of the VACNF-Sn based half-cell, significantly. It can be seen that first cycle coulombic efficiency is only ~ 69% which increases to ~94.5% in the second cycle and reaching ~97.8% after 50 cycles. Comparing with the literature (presented in Table I) the VACNF-Sn array anode shows good cycling stability at higher rate (C/3 rate). Thus, the addition of FEC in the electrolyte improve the capacity retention and coulombic efficiency, significantly.

CONCLUSIONS

In this work, we have investigated the electrochemical performance of the VACNF-Sn array electrode as a high performance lithium-ion battery anode. The VACNF-Sn array electrodes were prepared by sputter-coating Sn shells on VACNF cores. A high specific capacity of 815 mAh g^{-1} of Sn was obtained at C/20 rate in the initial cycles. The addition of FEC in the electrolyte improves the cycling performance of VACNF-Sn electrode significantly by enabling to form a stable solid electrolyte interface (SEI) layer. The VACNF-Sn array anode shows ~480 mAh g^{-1} capacity after 50 charge-discharge cycles at C/3 rate with FEC containing electrolyte.

ACKNOWLEDGMENTS

We gratefully acknowledge the financial support from the NASA MIRO Program No. NNX15AP44A and the National Science Foundation under Award No. 162-6449. JL acknowledges that the VACNF fabrication in this work was supported by a NSF grant DMR-1707585.

REFERENCES

[1] M. Winter, and J. O. Besenhard, *Electrochim. Acta* **45,** 31, (1999).
[2] C. K. Chan, H. Peng, G. Liu, K. McIlwrath, X. F. Zhang, R. A. Huggins, and Y. Cui, *Nat. Nanotechnol.* 3, 31 (2008).
[3] M. Zhao, Q. Zhao, J. Qiu, H. Xue, and H. Pang, *RSC Adv.* **6,** 95449 (2016).
[4] B. Wang, B. Luo, X. Li, and L. Zhi, *Materials Today* **15,** 544 (2012).
[5] L. Sun, X. Wang, R. A. Susantyoko, and Q. Zhang, *Carbon* **82,** 282 (2015).
[6] B. A. Cruden, A. M. Cassell, Q. Ye, and M. Meyyappan, *J. Appl. Phys.* **94,** 4070 (2003).
[7] A. V. Melechko, V. I. Merkulov, T. E. McKnight, M. Guillorn, K. L. Klein, D. H. Lowndes, and M. L. Simpson, *J. Appl. Phys.* **97,** 041301 (2005).
[8] S. A. Klankowski, G. P. Pandey, B. A. Cruden, J. Liu, J. Wu, R. A. Rojeski, and Jun Li, *J. Power Sources* **276,** 73 (2015).
[9] G. P. Pandey, S. A. Klankowski, Y. Li, X. S. Sun, J. Wu, R. A. Rojeski, and J. Li, *ACS Appl. Mater. Interfaces* **7,** 20909 (2015).
[10] D. Wang, X. Li, J. Yang, J. Wang, D. Geng, R. Li, M. Cai, T.-K. Sham, and X. Sun, *Phys. Chem. Chem. Phys.* **15,** 3535 (2013).
[11] Z. Yang, A. A. Gewirth, and L. Trahey, *Appl. Mater. Interfaces* **7,** 5667 (2015).
[12] S. Hong, M.-H. Choo, T. H. Kwon, J. Y. Kim and S.-W. Song, Adv. *Mater. Interfaces* **3,** 1600172 (2016).
[13] D. M. Seo, C. C. Nguyen, B. T. Young, D. R. Heskett, J. C. Woicik and B. L. Lucht, *J. Electrochem. Soc.* **162,** A7091 (2015).
[14] R. Tian, Y. Zhang, Z. Chen, H. Duan, B. Xu, Y. Guo, H. Kang, H. Li and H. Liu, *Sci. Rep.* **6,** 19195 (2016).
[15] Y. Dong, S. Das, L. Zhu, T. Ben and S. Qiu, *J. Mater. Chem. A* **4,** 18822 (2016).
[16] D.-H. Nam, J. W. Kim, J.-H. Lee, S.-Y. Lee, H.-A-S. Shin, S.-H. Lee, and Y.-C. Joo, J. Mater. Chem. A **3,** 11021 (2015).